An Interannual Study of the Atlantic North Equatorial Countercurrent*

ELI JOEL KATZ

Lamont–Doherty Geological Observatory, Columbia University, Palisades, New York

(Manuscript received 12 September 1991, in final form 30 March 1992)

ABSTRACT

Beginning in 1983, the dynamic height difference at the sea surface defining the countercurrent trough at 38°W was continuously observed by Inverted Echo Sounders at 3°N and 9°N for six years and ten months. The amplitude of the average annual signal for that time period was 36 cm, and the range of the interannual variability was 25 cm. Thus, the annual signal dominates as expected, but the interannual variability is of comparable magnitude. Two years, 1983 and 1987, are noted as years of sharp increase in the interannual signal (periods immediately following El Niño events in the Pacific). From a derived relationship for geostrophic volume transport, it is estimated that every year the North Equatorial Countercurrent attained a transport of 20 Sv ($\equiv 10^6$ m^3 s^{-1}) for at least one month, while in the cited years it sustained this value for over half the year. The output of an unbounded reduced-gravity model, forced by monthly averaged wind stress, is compared to the observations. The model can be tuned so that the observed annual variation is approximated but none of the interannual variability is captured by the analysis.

1. Introduction

In the dynamic sea surface topography of both tropical Atlantic and Pacific oceans is a nearly basinwide trough (Reid 1961; Merle 1978) that results in the North Equatorial Countercurrent (NECC), an eastward current flowing counter to the prevailing easterly trade wind. Taking advantage of long time records of sea surface height at selected Pacific islands, Wyrtki (1974) showed that interannual differences in the depth of the trough may be as large or larger than the seasonal difference. In the absence of such convenient islands in the Atlantic, estimates of the trough depth have been based on seasonal averages of all available data or on meridional hydrographic sections (Katz 1981). The latter were far too few to distinguish between annual and interannual variations but suggest a combined range of roughly 12–24 cm in the western Atlantic.

To separate and independently establish annual and interannual variations in the Atlantic, Inverted Echo Sounders were deployed at representative latitudes (3°N and 9°N) along the 38°W meridian from January 1983 into November 1989. Their locations relative to the mean dynamic topography are shown in Fig. 1, which suggests an average of 10–15-cm difference between them. In the next section the dataset is shown, its calibration established, and the general nature of the signal described.

About the time of the observations, two El Niño events occurred in the Pacific Ocean. Section 3 relates the interannual variations observed in the Atlantic to these events in the Pacific. This is followed by an estimate of the geostrophic transport implied by the sounder observations.

To explain the interannual variations of the countercurrent, one looks to the external forcing. What drives the countercurrent against the prevailing wind is the meridional shear of the zonal wind. Thus, one presumes that the observed interannual variations should be traceable back to variations in the wind field on the same time scale. A reduced-gravity model offers the simplest way of integrating the observed wind field to test this hypothesis, and in section 5 the results of such a calculation are compared to the observations.

2. Observations

The Inverted Echo Sounder (Bitterman 1976) is a spherically encased instrument that is deployed floating 1 m above the ocean floor and transponds and records the time for a 12-kHz signal to reflect off the ocean surface and return. In the application employed here, a burst sample of 20 signals was sent at 10-s intervals once an hour. Deployments were typically for about one year, and six deployments were necessary to achieve the record length (see Table 1). To join two records to obtain a continuous time series, the replacement sounder was deployed about 12 hours before the previous sounder was recovered. Spectra of the resulting time series are shown in Fig. 2.

The travel time is affected by two properties of the

* Lamont–Doherty Geological Observatory contribution 4921.

Corresponding author address: Dr. Eli Joel Katz, Lamont–Doherty Geological Observatory of Columbia University, Palisades, NY 10964.

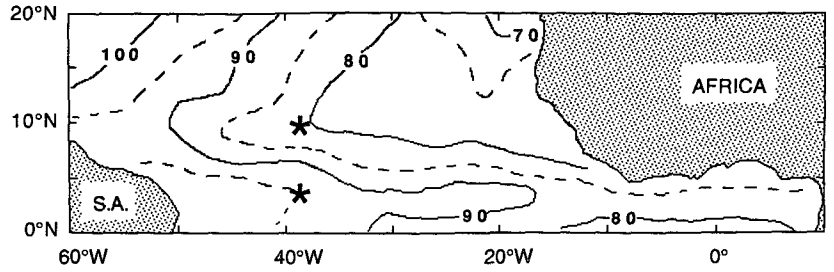

FIG. 1. Location of Inverted Echo Sounders. The two sounder sites are designated by stars on a map of the annual mean dynamic height (5 m relative to 500 m) derived from Merle (1978). Contours are every 5 cm.

ocean: changes in the height of the water column and changes in the sound velocity along the transmission path. The dominant process affecting the former are the tides, and these long records afford a unique opportunity to establish the amplitude and phase of many components. Table 2 describes several of the major constituents, where a nominal 1540 m s^{-1} sound velocity is used to convert travel time to sea surface amplitude.

A second high-frequency band (periods roughly of 2 to 5 days) of variance in the spectra is due to inertial gravity waves [previously described by Garzoli and Katz (1981) from earlier sounder records]. Before calibration, the high-frequency part of the signal is removed by a low-pass filter that essentially removes all energy below one cycle per 30 days and has a 50% amplitude reduction at 40 days (dashed lines in Fig. 2).

After filtering, the resulting time series of two-way travel times is interpreted as surface dynamic height relative to 500 db with the use of (i) an assumed value for the rate of change of travel time with dynamic height and (ii) an assigned value of the dynamic height for the mean travel time. The first is derived from historical data, and the value of 7.89 cm ms^{-1}, derived earlier (Katz 1987), is used. The mean dynamic height is obtained by comparing with data from hydrographic stations over the sounders during the deployment/recovery cruises. The result is shown in Fig. 3. For the two series, the standard deviation between sounder-derived dynamic height and observation is 3.0 cm at the two sites, combined.

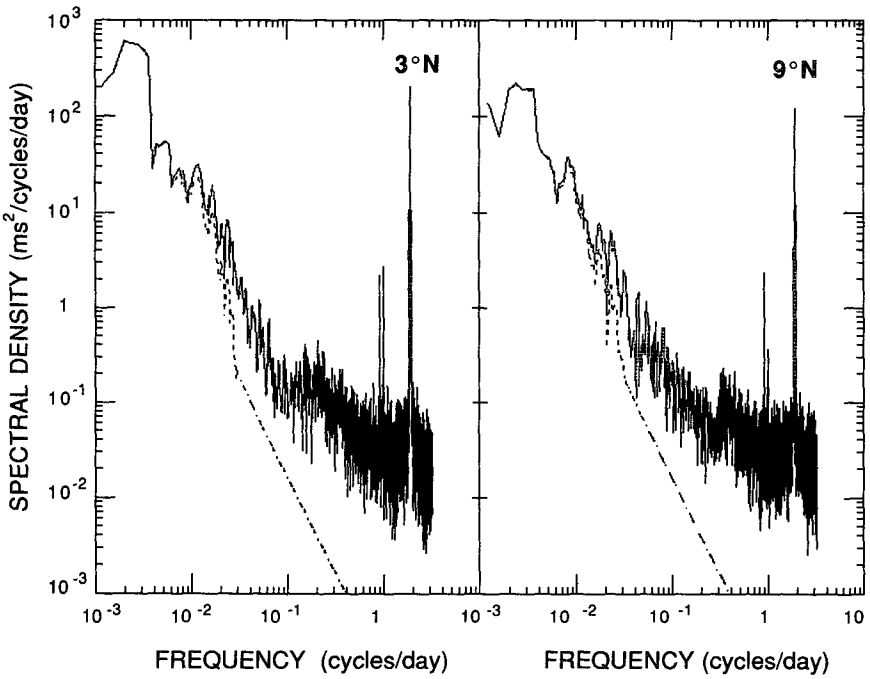

FIG. 2. Spectral density of sounder records. Units are milliseconds per cycle per day. Solid line is hourly data. Dashed line is after low-pass filter.

TABLE 1. Time and location of data records.

	Deployed (year day/year)	Recovered	Location (N)	Location (W)
I	35/83	252/83	9°01.0′	38°18.5′
II	252/83	291/84	9°04.5′	38°11.3′
III	291/84	304/85	9°04.4′	38°11.5′
IV	303/85	22/87	9°04.6′	38°11.4′
V	22/87	164/88	9°05.1′	38°11.2′
VI	164/88	312/89	9°08.2′	38°04.2′
I	37/83	250/83	3°03.0′	38°34.0′
II	250/83	293/84	3°17.2′	38°34.8′
III	293/84	302/85	3°17.0′	38°35.5′
IV	301/85	20/87	3°15.9′	38°35.5′
V	19/87	161/88	3°16.1′	38°36.8′
VI	161/88	310/89	3°15.8′	38°37.2′

Of interest is the difference in dynamic height between the two sites that straddle the NECC. This is shown in Fig. 4 and reflects the anticipated spring/summer buildup of the countercurrent and its fall/winter relaxation. The mean difference, 15 cm, is close to the historical average derived from Fig. 1.

To quantify the separate contributions of annual and interannual variations, a six-year climatology is derived from the dataset and shown in Fig. 5. The climatology at the individual sites are roughly 180 degrees out of phase, with the larger part of the signal coming from 3°N (a range of 30 cm, compared to 12 cm at 9°N).

In the absence of interannual variations, the climatology would suggest the absence of a countercurrent in March and April and a maximum countercurrent from August through November. The range is −6 to +30 cm. Richardson and Walsh (1986) plotted four monthly maps of surface current from historical ship-drift reports. Along 38°W, their maps are consistent with this timing of the annual cycle. They show weak westward current in February and May, contrasting to eastward current in August and November. Merle (1978) plotted two three-month averages of dynamic height (5 m Re 500 m) from available hydrographic data. Along 38°W, between 9°N and 3°N, they showed a similar result. In January–March there is a difference

TABLE 2. Principle tidal constituents.

Location:	9°04.73′ N 38°11.35′ W		3°14.17′ N 38°35.63′ W	
Constituent	Amplitude (cm)	Phase (deg)	Amplitude (cm)	Phase (deg)
Q_1	0.97	195.17	0.94	210.76
O_1	6.39	241.95	6.15	221.21
P_1	0.84	265.03	1.50	292.24
K_1	2.27	269.41	7.20	270.71
N_2	9.94	210.95	16.50	219.86
M_2	55.38	221.12	73.57	235.15
S_2	16.49	251.89	16.22	248.77
K_2	4.94	257.83	6.31	244.28

Notes: 1) Tidal analysis performed with G. Godin's tidal current analysis and prediction computer programs (see Pacific Marine Science Reports 77-10, 78-6, and 79-15, by Foreman et al.). The "standard" table of 69 constituents was used.

2) Location is an average of the sequential deployments. No adjustments are made for positional variations (see Table 1).

3) All data are from "hourly" samples. Clock drift in a year's deployment was typically ten minutes and each segment was linearly interpolated to on the hour before analysis.

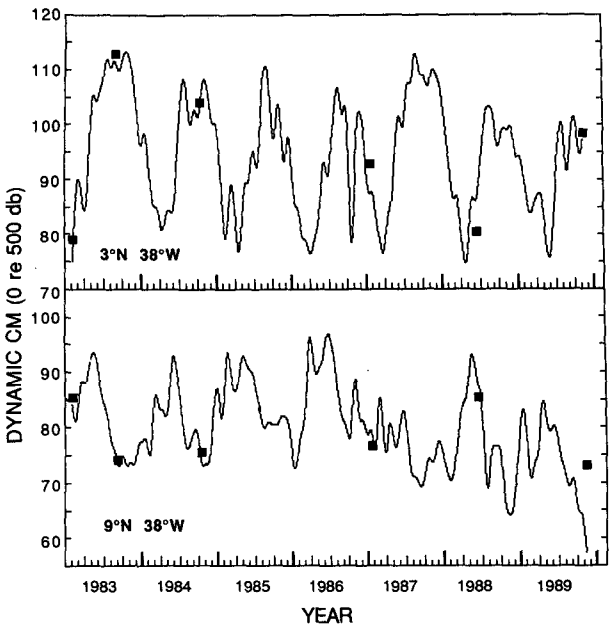

FIG. 3. Dynamic height of low-frequency sounder records and CTD calibration data. CTD data, shown as rectangles, were obtained during deployment cruises. The 1989 data point at 9°N was excluded from analysis as an outlier.

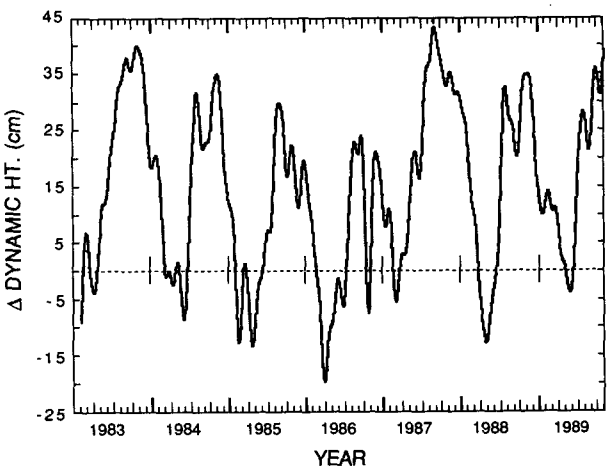

FIG. 4. Difference in dynamic height between the two sounders. Data is the difference of the two panels in Fig. 3.

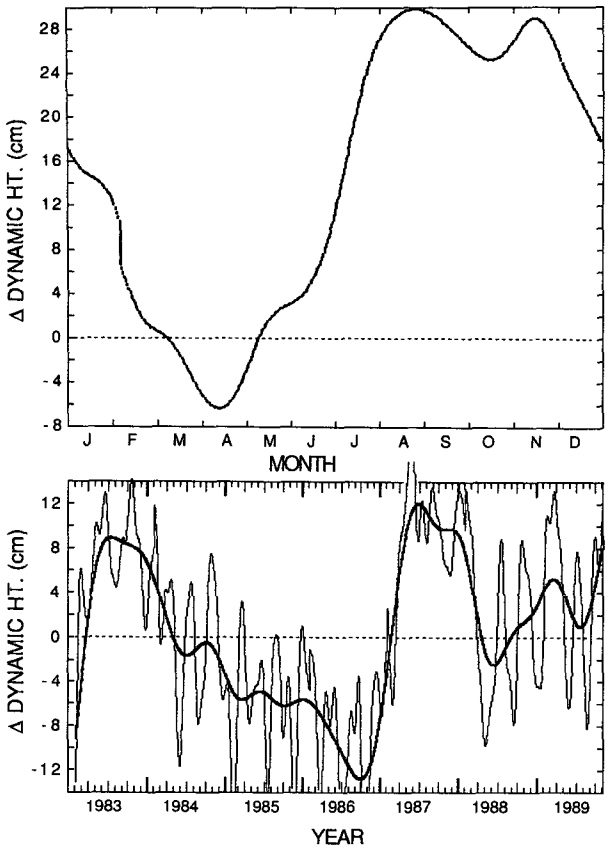

FIG. 5. Climatology (upper panel) and interannual anomaly (lower panel) of the sounder's height difference. With the change in scale the interannual signal "looks noisy," and the solid line is after filtering the interannual signal again with the same low-pass filter as before. Subsequent discussion is about this twice-filtered signal.

of 7 cm, while in July–September it is 24 cm, in rough agreement with the sounder result.

3. Relation to El Niño

Having found that the climatology based on a relatively short period is comparable to other previous views of the annual cycle, which contain data over longer periods (albeit nonuniformly distributed), the anomaly signal shown in Fig. 5 can be thought of as qualitatively representative. The interannual variability is 25 cm, or two-thirds of the annual variation.

During the six years there are two distinct periods of sharp and sustained increase in the interannual signal: the first half of 1983 and 1987, with a nearly monotonic decrease between them and an arrested decrease after 1987. The former two years are periods following exceptional surface winds in the Pacific Ocean, known as El Niño (Philander 1990). In Fig. 6 the Southern Oscillation index (SOI) is compared to the interannual variation of the NECC.

To make this comparison, both are shown as standard deviations about their means. The SOI data, based on the atmospheric surface pressure difference between Tahiti and Darwin, were provided by Vernon Kousky and are an update of the time series described by Chelliah (1990). It has been smoothed over a five-month band to make it comparable to the NECC data. Minimum values of the SOI are indicative of minimum trade winds across the Pacific and a maximum in convective activity in the central and eastern sectors (Rasmusson and Wallace 1983). The latter presumably affects the global atmospheric circulation.

In the six-year record of the NECC index there are two maxima of about 1.5 and 2.0 standard deviations, and they both occur about one-half year or less after the two minima in the SOI (with the hint of a third event developing as our record runs out). The midyears between the two events are featureless in both signals.

4. Geostrophic transport

While it is relatively obvious that the sea surface height differential across the NECC is a qualitative measure of its geostrophic strength, it would be better if this could be made quantitative. While there need not be a unique relationship between height difference and mass transport, in an earlier work (Katz 1981, Fig. 4) a correlation between the two was shown from an analysis of nine historical meridional sections between 25° and 35°W. The result was a near-square-root dependency of geostrophic transport versus height difference. These data are shown in Fig. 7, with two additional data points from the 1987 and 1989 cruises along 38°W deploying the sounders.[1] Station spacing was one degree or less and the transport is from surface to the 500-db reference level. A linear regression, shown in the figure, yields the relation

$$\text{transport (in Sv)} = 4.2 * \sqrt{\text{delta ht. (in cm)}},$$

with a standard error of 3.4 Sv (1 Sv $\equiv 10^6$ m^3 s^{-1}).

From this, a continuous estimate of the geostrophic transport of the countercurrent can be derived from Fig. 4. This is shown in Fig. 8 for monthly averages. The range of peak annual values is relatively limited, only varying between 20 and 27 Sv. The total annual transport (i.e., the integral under the curve for each annual cycle of the countercurrent) has a much larger interannual variation: threefold in the extreme comparison between 1986 and 1987. The standard deviation of the annual geostrophic flow (for 1983–89) is 30% of the mean.

[1] In 1988 a transport of 0.6 Sv was calculated, and the height difference was a negative 4.7 cm. This point is not included in the analysis. The years 1983 and 1984 are not included, as there were insufficient data to compute transport between the sounder sites.

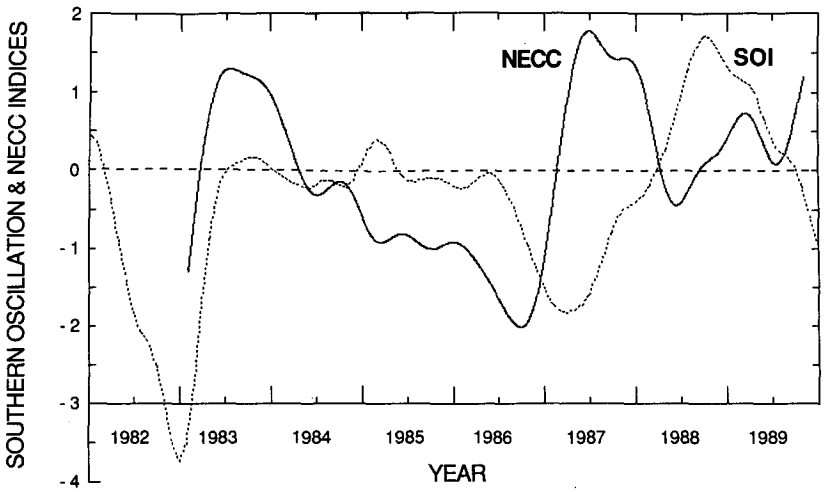

FIG. 6. Comparison between North Equatorial Countercurrent and Southern Oscillation indices. The ordinate is in terms of each series' standard deviation. Source and smoothing of the SOI data are discussed in text.

5. Reduced-gravity model calculation

The interannual variation in the NECC is most likely attributable to the interannual variation in the surface wind field. It is, however, an integrated effect in both space and time. It would be insufficient, for example, to directly compare the ocean observations with the wind field at 38°W.

A model is needed to integrate the observed winds downwind until 38°W, and the simplest model is a two-layered reduced-gravity model (Busalacchi and O'Brien 1980, in the Pacific; Busalacchi and Picaut 1983, in the Atlantic). To focus solely on the direct effect of the wind stress, we simplify even further by considering the ocean as unbounded to the west. As described in Katz (1987), after ignoring higher-order acceleration terms and the meridional wind stress, we numerically solve the equations:

$$\frac{\partial h}{\partial t} - c\frac{\partial h}{\partial x} = \frac{1}{f\rho}\frac{\partial \tau_x}{\partial y} - \frac{1}{f\rho y}\tau_x$$

with

$$c = \beta\frac{\Delta\rho}{\rho}g\frac{h}{f^2}, \quad \tau_x = \rho_a C_D \mathbf{V}_x|\mathbf{V}|, \quad \eta = \frac{-\Delta\rho}{\rho}h,$$

where η is sea surface height, h is the thermocline depth, x and y are east and north (with $y = 0$ at the equator), $f(=\beta y)$ is the Coriolis parameter, ρ and ρ_a are water and air density, $\Delta\rho$ is the density difference between the two ocean layers, τ_x is the wind stress on the surface,

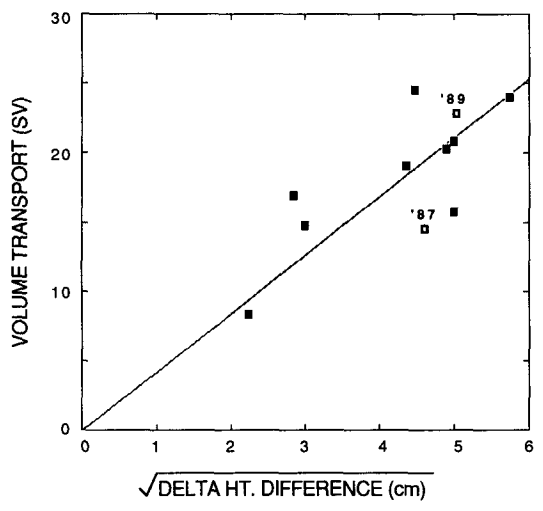

FIG. 7. Geostrophic volume transport compared to the difference in dynamic sea surface height. Both transport and height are between 3° and 9°N and are relative to 500 dbars. Solid boxes are from Katz (1981). The line is from a linear regression with no constant (coefficient of correlation: .71).

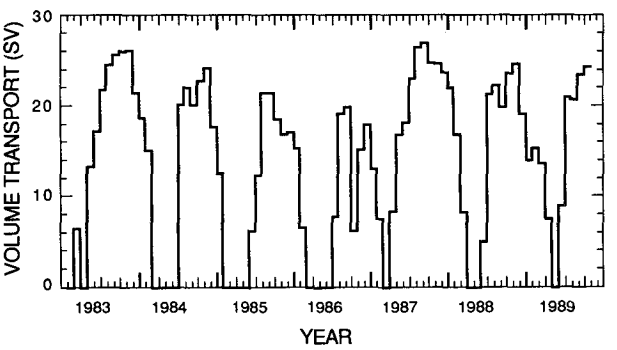

FIG. 8. Monthly averaged eastward geostrophic volume transport. The data of Fig. 4 are averaged and converted to transport using the regression shown in Fig. 7. Zero transport is plotted when the monthly dynamic height at 9°N exceeds that at 3°N.

V is the observed wind above the sea surface, and C_D is the drag coefficient. In the calculations $\rho_a = 1.2 \times 10^{-3}$ g cm^{-3}, $\Delta\rho/\rho = 4.0 \times 10^{-3}$, and $C_D = 1.5 \times 10^{-3}$. As described in the earlier work, the density difference between the two layers is derived from a linear regression of dynamic height on thermocline depth from monthly averaged climatological data.

The calculation is done separately along 3°N and 9°N, beginning at 20°W [chosen because the annual harmonic of the surface dynamic height is climatologically a minimum there (Merle and Arnault 1985)] and integrating westward in two-degree intervals. Updated monthly averages of the wind field were provided by J. Servain from an objective analysis of ship-reported wind (Servain et al. 1985). The data are reduced to a 2° × 2° grid; thus, the meridional derivative of wind stress is computed over 4°.

The initial condition is a flat sea surface above a constant thermocline depth of $h = 50$ m. The latter is the mean annual depth along 20°W between the two latitudes. At 20°W h remains constant, but to the west it changes to reflect changes in sea surface height. The calculation begins in January 1982, or one year before the ocean observations. In Katz (1987, Figs. 11 and 12), it is shown that the change in surface height at each site results from a near balance of the opposing forces with the timing of the seasonal changes being controlled by the time of increasing and decreasing meridional wind shear stress. Subtracting the two calculations yields a daily time series of the difference in dynamic height along 38°W. This is then smoothed and analyzed the same way as was done for the sounder data, and the resulting climatology and anomaly is shown for both in Fig. 9.

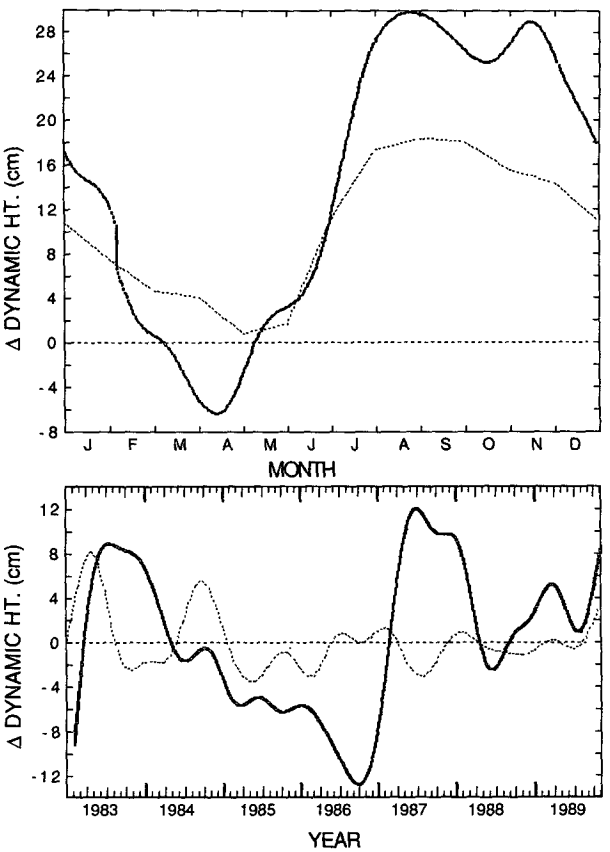

FIG. 9. Comparison of climatology and interannual anomaly between sounder data and reduced-gravity model. Data is the solid line (from Fig. 5); model is the dashed line.

The model climatology shows the seasonal difference between weak slope in the spring contrasted to a maximum in the summer, but has a reduced range of about half that of the data. The discrepancy between model and data is most noticeable when considering the anomaly signal (Fig. 9, lower panel). None of the interannual variability is reflected in the model results.

A series of sensitivity runs were made varying the initial thermocline depth and the drag coefficient. The model is relatively insensitive to the former but, as can be seen in Fig. 10, doubling the drag coefficient increases the range of the model climatology and aside from missing the slope reversal in the spring, tracks the data quite well. Changing the drag coefficient, however, does not improve the model's inability to reproduce any feature of the interannual record.

To attempt to shed some light on where the model most diverges from the observations, the climatology and interannual anomaly at each latitude are compared in Fig. 11 (the drag coefficient set at its unexaggerated value of 1.5×10^{-3}). The climatological comparisons find the model predicting the range and phase of the observations rather well at 3°N and not at all at 9°N (up to an arbitrary constant that is added to the model results at both latitudes). The discrepancy between model and observation of the interannual anomaly is poor at both latitudes, but is relatively worse at 9°N. At 3°N the model at least shows the correct time derivative more often than not. Thus, while the model results are not encouraging at either latitude, it would appear that the comparative results between them are uneven.

6. Discussion

The comparison of model output to data leads to the following conclusion. Since the annual variation is larger than the interannual variance, any model that can reproduce the phase of the annual variance can be tuned to closely approximate one year, or even several nonexceptional years, of data. That leaves the interannual variance as the test of a model and its input. Therefore, in the equatorial Atlantic, where long time in situ measurements have not been easily obtained, model validation is presently very limited. The satellite altimeter (e.g., Carton and Katz 1990), however, may alter this situation in the present decade.

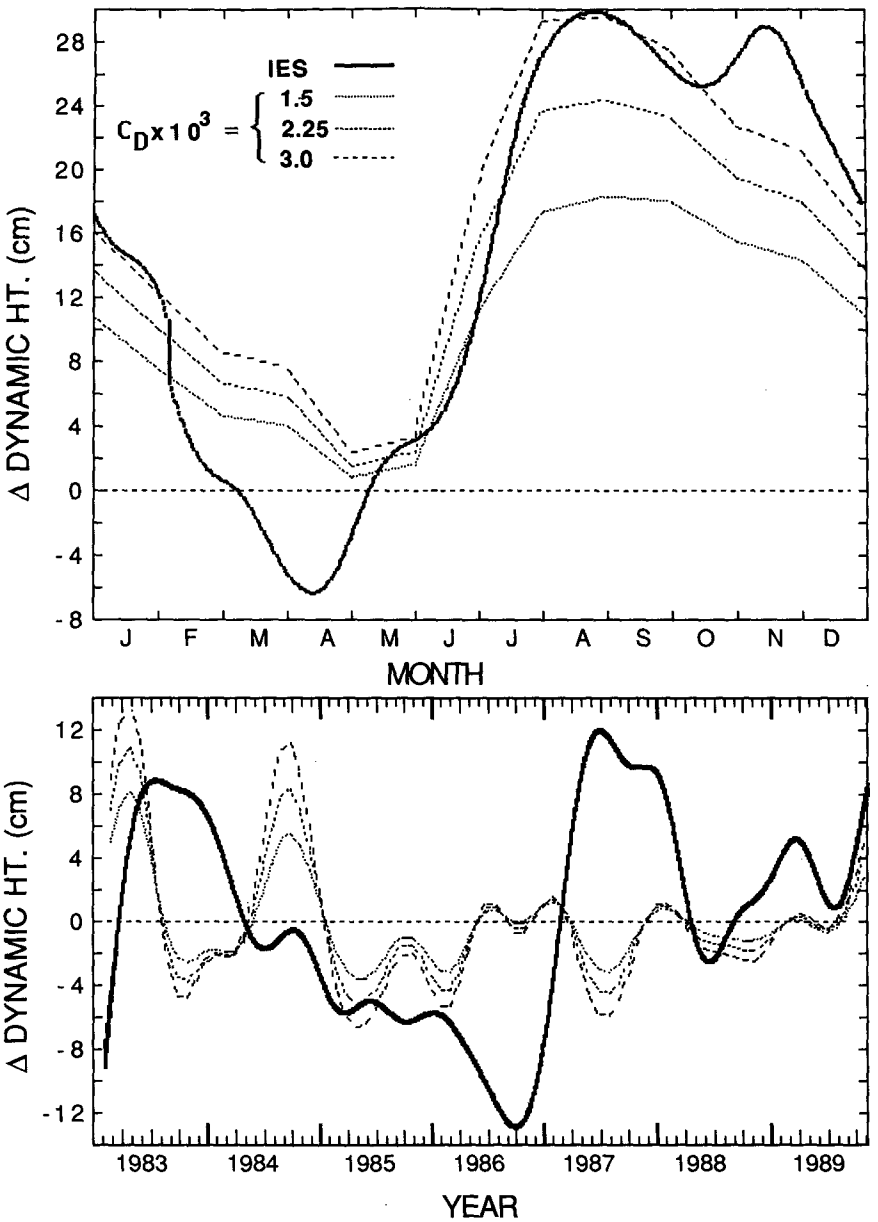

FIG. 10. Same as Fig. 9 with varying drag coefficient.

The dataset from the sounders presented here is unique at this time, but it still represents only one aspect (or one dimension) of the circulation. The inability of the unbounded reduced-gravity model to reproduce the interannual variation can arise either from the assumptions of the model or the inadequacy of the wind field forcing the model to accurately describe the forcing, or both. Assuming that the wind field is adequate, then the conclusion is that a simple downwind integral of the relevant yearly wind stress does not identify years of anomalous sea surface variability.

The absence of a western boundary in the model is most likely primarily responsible for the lack of an acceptable interannual simulation. If this proves to be the case, then what has been demonstrated by this exercise is that, not surprisingly, the interannual variance is due to the closed basinwide response to the wind field. S. Zebiak has made some preliminary calculations for the years of the sounder data with the model described by Cane and Pattern (1984) [and previously applied to the Pacific by Zebiak and Cane (1987)] and plans to report on this work in the future.

Beyond the present model's deficiency, the poor sampling provided by ship observations forces a smoothing of the wind field, which could conceivably partially mask interannual variations in the basinwide

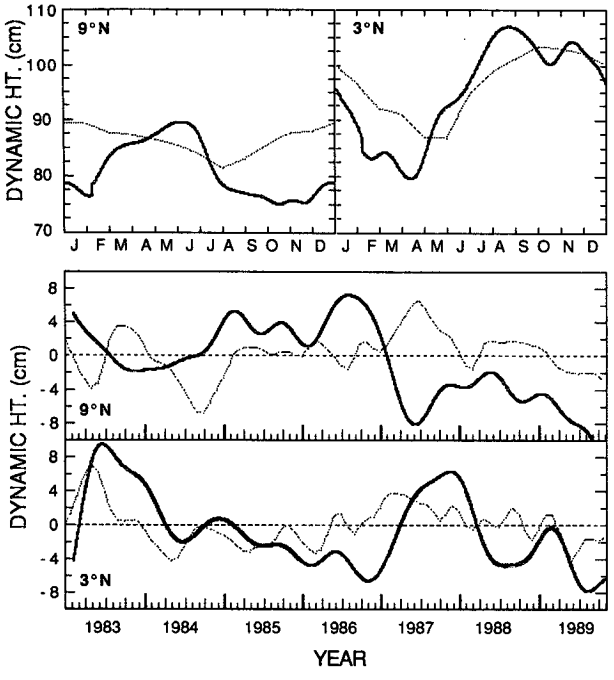

FIG. 11. Comparison of climatology and interannual anomaly between sounder data and model (dashed lines) at 9°N, 38°W and 3°N, 38°W.

integrated wind field. This situation will remain until satellite-derived sea-surface wind fields become routinely available.

While a seven-year record length is still relatively short to discuss interannual variations, it nonetheless did contain two "events" of increased interannual signal. These occur in years following El Niño events in the equatorial Pacific and, without being specific about the exact mechanisms involved, it is reasonable to speculate that upper-atmospheric changes associated with the increased convection in the Pacific affect the trade winds over the Atlantic. Philander (1990) discusses this connection when noting the strong Atlantic trade winds in the year following the 1982 El Niño.

The result of a deepening countercurrent trough is an increase in the annual eastward transport of the North Equatorial Countercurrent. Without interannual variation, we estimate an average transport of 20 Sv for five months of the year (from mid-July through mid-December). In contrast, in the years following El Niño events in the Pacific, transports exceeding 25 Sv are sustained for that period, or longer.

Acknowledgments. The acquisition of the data reported here was funded by the National Science Foundation under Grants OCE 81-17000 and OCE 84-15319. The analysis was completed with assistance from NOAA Contract NA89-AA-D-ACO67. Sounder deployments and recoveries were made during the research cruises CONRAD 24-01 and 29-06; ENDEAVOR EN-136, -205; and GYRE 84 G11. The instrumentation was initially maintained by Esteben Draganovic, and then by Miguel Maccio for most of the period. A succession of programmers worked on the data, with the final work being done by John Webber. Finally, I wish to acknowledge discussions with Drs. Steve Zebiak and Yves Tourre who made important comments while the work was in progress.

REFERENCES

Bitterman, D. S., Jr., 1976: Inverted Echo Sounder instrument report. Woods Hole Oceanographic Institute. Tech. Rep., Ref. No. 76-67,

Busalacchi, A. J., and J. J. O'Brien, 1980: The seasonal variability in a model of the tropical Pacific. *J. Phys. Oceanogr.*, **10,** 1929–1951.

——, and J. Picaut, 1983: Seasonal variability from a model of the tropical Atlantic Ocean. *J. Phys. Oceanogr.*, **13,** 1564–1588.

Cane, M. A., and R. J. Patton, 1984: A Model of El Niño–Southern Oscillation. *Mon. Wea. Rev.*, **115,** 2262–2278.

Carton, J. A., and E. J. Katz, 1990: Estimates of the zonal slope and seasonal transport of the Atlantic North Equatorial Countercurrent. *J. Geophys. Res.*, **95,** 3091–3100.

Chelliah, M., 1990: The global climate for June–August 1989: A season of near normal conditions in the tropical Pacific. *J. Climate,* **3,** 138–162.

Garzoli, S. L., and E. J. Katz, 1981: Observations of inertia–gravity waves in the Atlantic from inverted echo sounders during FGGE. *J. Phys. Oceanogr.*, **11,** 1463–1477.

Katz, E. J., 1987: Seasonal response of the sea surface to the wind in the equatorial Atlantic. *J. Geophys. Res.*, **92,** 1885–1893.

——, 1981: Dynamic topography of the sea surface in the equatorial Atlantic. *J. Mar. Res.*, **39,** 53–63.

Merle, J., 1978: Atlas hydrologique saisonnier de l'océan Atlantique intertropical. Travaux et Documents de l'O.R.S.T.O.M. No. 82, 184 pp.

——, and S. Arnault, 1985: Seasonal variability of the surface dynamic topography in the tropical Atlantic Ocean. *J. Mar. Res.*, **43,** 267–288.

Philander, S. G., 1990: *El Niño, La Niña, and the Southern Oscillation.* Academic Press. 293 pp.

Rasmusson, E. M., and J. M. Wallace, 1983: Meteorological aspects of the El Niño/Southern Oscillation. *Science,* **222,** 1195–1202.

Reid, J. L., 1961: On the geostrophic flow at the surface of the Pacific Ocean with respect to the 1,000-decibar surface. *Tellus,* **13,** 489–502.

Richardson, P. L., and D. Walsh, 1986: Mapping climatological seasonal variations of surface currents in the tropical Atlantic working ship drifts. *J. Geophys. Res.*, **91,** 10 537–10 550.

Servain, J., J. Picaut, and A. J. Busalacchi, 1986: Interannual and seasonal variability of the tropical Atlantic Ocean depicted by sixteen years of sea-surface temperature and wind stress. *Coupled Ocean–Atmosphere Models,* J. C. J. Nihoul, Ed., Elsevier Science, 211–237.

Wyrtki, K., 1974: Equatorial currents in the Pacific 1950 to 1970 and their relations to the trade winds. *J. Phys. Oceanogr.*, **4,** 372–380.